PNAS RESEARCH ARTICLE | APPLIED PHYSICAL SCIENCES

Collective chemomechanical oscillations in active hydrogels

Baptiste Blanc[a,b,c,1], Johnson N. Agyapong[c,d], Ian Hunter[c], Jean-Christophe Galas[a], Alberto Fernandez-Nieves[b,e,f], and Seth Fraden[c]

Edited by Monica Olvera de la Cruz, Northwestern University, Evanston, IL; received August 2, 2023; accepted November 14, 2023

We report on the collective response of an assembly of chemomechanical Belousov-Zhabotinsky (BZ) hydrogel beads. We first demonstrate that a single isolated spherical BZ hydrogel bead with a radius below a critical value does not oscillate, whereas an assembly of the same BZ hydrogel beads presents chemical oscillation. A BZ chemical model with an additional flux of chemicals out of the BZ hydrogel captures the experimentally observed transition from oxidized nonoscillating to oscillating BZ hydrogels and shows this transition is due to a flux of inhibitors out of the BZ hydrogel. The model also captures the role of neighboring BZ hydrogel beads in decreasing the critical size for an assembly of BZ hydrogel beads to oscillate. We finally leverage the quorum sensing behavior of the collective to trigger their chemomechanical oscillation and discuss how this collective effect can be used to enhance the oscillatory strain of these active BZ hydrogels. These findings could help guide the eventual fabrication of a swarm of autonomous, communicating, and motile hydrogels.

chemomechanics | reaction–diffusion | nonlinear dynamic

Significance

Living organisms directly transform chemical energy at the molecular scale into coordinated motion up to the multiorganism scale. Such coordination across scales can be mediated by chemical communication. An example accessible to all is ants that use chemical signaling to drive their self-organization for optimized food foraging. Synthetic materials that harness autonomously chemical energy from their environment to generate chemical communication and actuate are rare. Combining theory and experiment, we show that Belousov-Zhabotinsky hydrogels present collective chemical behavior that can be used to trigger their chemomechanical oscillation. Our findings are important for optimizing the performance of autonomous chemomechanical machines and for building adaptive life-like materials.

Numerous phenomena in living systems, such as fish schooling (1), the heart beat (2), the cytoskeleton transport (3), or the flocking of cells (4, 5) are collective ones, stemming from the local interactions of many mechanically active units (6, 7). In particular, yeast and other unicellular organisms spatially aggregate when, for example, nutrients are lacking in the media (8, 9). This behavior at the scale of the organism is induced by the production of chemicals at the cellular scale, which propagates over the entire system through spatial coupling by diffusion. The resulting reaction–diffusion transport on macroscopic lengths appears in the form of propagating waves. This mode of chemical communication between cells, known as quorum sensing, allows the cells to move toward each other and self-assemble into patches of high density (10).

There have been recent works demonstrating that synthetic materials composed of rigid particles such as micrometric porous particles loaded with the Belousov-Zhabotinsky (BZ) oscillator or a DNA–enzyme oscillator can emulate the collective chemical response shown by living organisms (11–15). However, these rigid particles are nonresponsive and hence would not aggregate into patches when their quorum sensing becomes active. To observe self-assembly, an actuation mechanism that could result in a mechanical response of these particles is necessary and has yet to be demonstrated.

In this article, we show that the chemical quorum sensing of soft BZ oscillating hydrogels triggers their mechanical oscillation, elucidating a mechanism by which aggregation could be achieved. The simplest description of the BZ hydrogel mechanism consists in separating the BZ chemical reaction from its actuation. In the BZ reaction, an autocatalytic activator drives the catalyst to its oxidized state and generates an inhibitor that returns the catalyst to its reduced state (16). The cyclic change of the oxidation state of the catalyst induces the oscillatory swelling of the hydrogel (17, 18). We first establish that a single isolated spherical BZ hydrogel smaller than a critical size never oscillates when immersed in a large volume of uncatalyzed BZ solution. Both the experiment and the theory indicate that this size-dependent behavior is due to a competition between the reaction kinetics of the inhibitor of the BZ reaction and its transport to the outer solution. We then study the chemical oscillation of an assembly of close-packed BZ hydrogel beads. We observe that BZ hydrogel beads, with a radius smaller than the previously established critical size for a single isolated BZ hydrogel to oscillate, sustain chemical activity for days. We show that this phenomenon is robust and does not depend on the properties of the BZ hydrogel beads, its catalyst concentration, or its elasticity. By tuning the BZ hydrogel composition in order to increase its mechanical oscillation, hydrogels smaller than the critical size are made mechanically active. Finally, we discuss why this finding is important for optimizing the performance of metabolic chemomechanical machines, paving the way to the creation of the model system, recently called "swarmalator," consisting of a swarm of autonomous chemomechanical oscillating actuators (19).

Author contributions: B.B. and S.F. designed research; B.B. and J.N.A. performed research; I.H., J.-C.G., A.F.-N., and S.F. contributed new reagents/analytic tools; J.-C.G. and A.F.-N. reviewed and edited the paper; B.B. analyzed data; and B.B. wrote the paper.

The authors declare no competing interest.

This article is a PNAS Direct Submission.

[1]To whom correspondence may be addressed. Email: baptiste.blanc@sorbonne-universite.fr.

This article contains supporting information online at https://www.pnas.org/lookup/suppl/doi:10.1073/pnas.2313258121/-/DCSupplemental.

Published February 1, 2024.

1. Chemical Oscillation of Single BZ Hydrogel Beads

BZ hydrogel beads loaded with the BZ Ruthenium catalyst [$(Ru(bpy)_2(bpyEtAm)(PF_6)_2)$] are placed into a container of 1 cm in diameter and 5 mm in height, covered with catalyst-free BZ reaction solution, and monitored from above with a digital camera (Fig. 1*A*). BZ hydrogel beads of radii ranging from $\sim$ 10 to 400 μm are synthesized following recent procedures (*Materials and Methods*, A and B) (18, 20). We first create hydrogel beads that are then functionalized with a homemade BZ Ruthenium catalyst. Monodisperse hydrogel beads with tunable concentration of polymer and catalyst are synthesized from a molding technique. Polydispersed hydrogel beads are created from an emulsion polymerization method, allowing fast production of a large number of hydrogel beads with a broad size distribution (21). The resultant radius distribution is fitted with a Gaussian function, with a mean radius of 73 μm and a SD of 28 μm (*SI Appendix*, section 2). Here, we use BZ hydrogel beads that have a Ruthenium catalyst concentration $c_{Ru^{2+}}$ ranging from 3 to 30 mM, and a polymer concentration c_{pol} ranging from 20 to 80 kg m^{-3}. The solution of BZ reactant is kept at the following constant concentrations [H_2SO_4] = 0.4 M, [$NaBrO_3$] = 0.08 M, [MA] = 0.06 M, corresponding to a chemical composition widely used for BZ chemomechanical hydrogels. Unless mentioned otherwise, the container is made of a glass slide at the bottom and top, with a PDMS lateral wall of a few millimeters in height and a centimeter in diameter. The solution is kept under pressure with a clamp to avoid evaporation and the creation of carbon dioxide bubbles (Fig. 1*A*). With this setup, we record the change in color of the catalyst and the radius change of the BZ hydrogel as a function of time (Fig. 1 *C* and *D*).

We find that single BZ hydrogel beads do not chemically oscillate when their radius is below a critical radius $R_{c,exp} = (225 \pm 9)$ μm (Fig. 1*B*). For a BZ hydrogel bead with a radius below $R_{c,exp}$, the catalyst in the BZ hydrogel stays oxidized (Fig. 1*C*). For a BZ hydrogel bead with a radius above $R_{c,exp}$, the BZ hydrogel first oscillates with a long period of oscillation and transitions either to a state with a shorter steady period of oscillation or die (Fig. 1*D* and *SI Appendix*, section 4). The transition from a long period of oscillation to a shorter and steady period of oscillation occurs through a transient birythmic regime where both frequencies (long and short) are present. We also find that the critical radius $R_{c,exp}$ does not show a significant variation with the catalyst concentration in the BZ hydrogel bead (*SI Appendix*, section 3).

2. Collective Chemical Oscillation of BZ Hydrogel Beads

To examine how the presence of neighboring BZ hydrogel beads affects their oscillation, we first place a collection of close-packed BZ hydrogel beads with a broad radius distribution in a microfluidic chamber through which we flow the surrounding uncatalyzed BZ solution. We observe that chemical waves of reaction–diffusion propagate in such a divided medium for

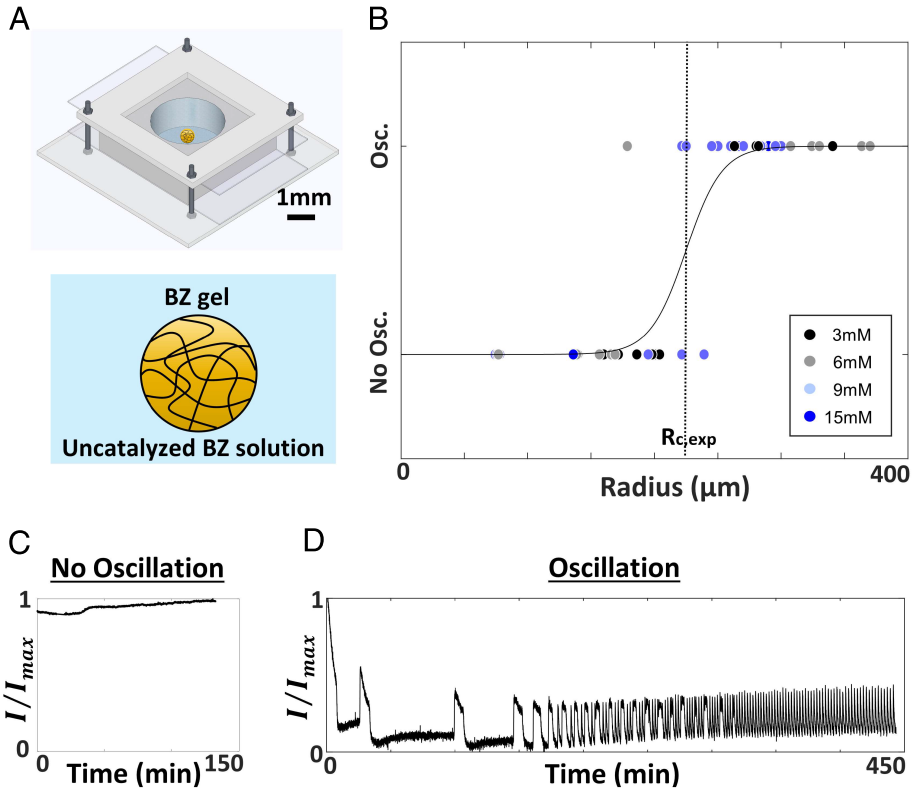

Fig. 1. Experiments on the chemical oscillation of single BZ hydrogel beads. (*A*) Schematic of the experimental setup. (*B*) Classification of the gel in oscillating state (Osc.) and nonoscillating oxidized state (No Osc.) as a function of its radius for various BZ hydrogel beads compositions. The color code for the data points stands for the ruthenium catalyst concentration in the BZ hydrogel bead. The dark line represents the probability of being oxidized or oscillating as a function of the BZ hydrogel bead radius for all the composition of BZ hydrogel beads. We define the critical radius $R_{c,exp}$ as the radius at which the probability for a BZ hydrogel bead to oscillate is $\frac{1}{2}$. We find $R_{c,exp} = (225 \pm 9)$ μm with the error bar corresponding to a 95% CI. (*C*) Intensity as a function of time of a BZ hydrogel bead with a radius below $R_{c,exp}$. The gel stays oxidized. (*D*) Intensity as a function of time of a BZ hydrogel bead with a diameter above $R_{c,exp}$. For some BZ hydrogel beads, the oscillation stops before reaching the regime of steady state oscillation (*SI Appendix*, section 4).

days (Movie S1). Therefore, BZ hydrogel beads smaller than the critical size $R_{c,exp}$ can chemically oscillate when surrounded by others. We then assemble quasi-2D layers of BZ hydrogel beads in the chambers we used for the single BZ hydrogel bead experiments (Fig. 1*A*). Chemical waves of reaction–diffusion are also observed in these 2D media. BZ hydrogel beads as small as $\frac{R_{c,exp}}{10} \approx 20\,\mu m$ in radii show sustained chemical oscillations (Fig. 2*A*). We note that the measured lower size for a BZ hydrogel bead to oscillate is due to the resolution of our optical setup. We also note that quasi-2D layers of BZ hydrogels beads all individually smaller than the critical size for an isolated BZ hydrogel bead to oscillate also support chemical oscillations (Fig. 2*B* and Movie S2). These experimental results are reminiscent of prior works demonstrating the existence of quorum sensing for BZ microreactors. Oscillating micrometric porous particles loaded with the BZ catalyst dispersed in a solution of uncatalyzed BZ solution have been shown to oscillate in synchrony when strongly stirred (11). The intermediate products generated by the BZ reaction inside the particles diffuse to the outer solution. When stirring is sufficiently strong, the concentration of these mobile chemical species is homogeneous in the uncatalyzed BZ solution. These chemical intermediates mediate the synchronous oscillations of the BZ microreactors. Monolayer made of excitable BZ micrometric particles in a solution of uncatalyzed, unstirred BZ solution has also been found to oscillate as a quorum (12–14). Through numerical simulations, the authors showed that this collective behavior is correlated with a decrease of the activator loss rate averaged over the entire BZ microreactor assembly. In all these previous works and in contrast to our experiments, the BZ microreactors are rigid, hence not mechanically responsive, homogeneous in catalyst concentration and in size, and stay reduced when not oscillating.

To characterize the chemical oscillations in BZ hydrogel beads of various sizes and concentrations of catalyst, we add a few BZ hydrogel beads of specific size and catalyst concentration to a quasi-2D layer of polydispersed BZ hydrogel beads with low catalyst concentration (3 mM) (Fig. 2*B*). We find that the critical size for a BZ hydrogel bead to oscillate disappears independently of its catalyst concentration (Fig. 2*A*). Similarly to what we observe with single BZ hydrogel beads, the BZ hydrogel beads experience a transient regime with a long period of oscillation, which then stabilizes to a steady-state regime of oscillation with a constant period (*SI Appendix*, section 5). The steady-state regime of oscillation, the period of chemical oscillation is found to increase with the catalyst concentration in the BZ hydrogel beads (Fig. 2*C*).

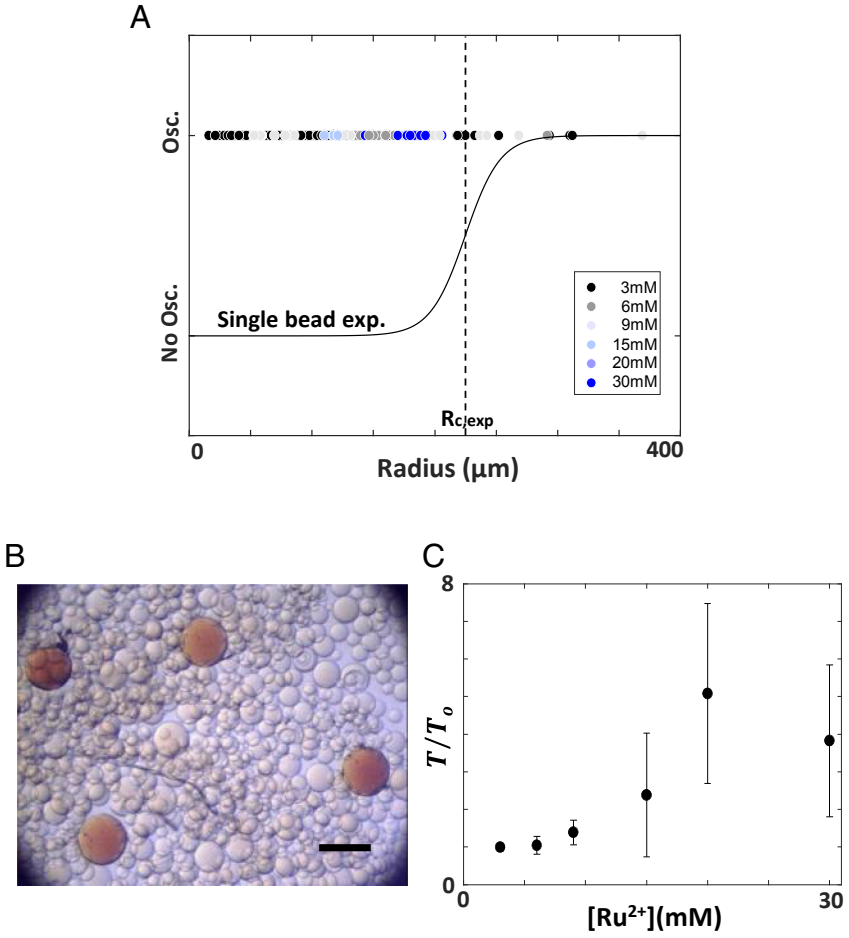

Fig. 2. Experiments on the collective chemical oscillation of BZ hydrogel beads. (*A*) Classification of the BZ hydrogel bead in oscillating state (Osc.) and nonoscillating oxidized state (No Osc) as a function of its radius for various BZ hydrogel bead compositions. In dark, probability of being oxidized or oscillating as a function of the BZ hydrogel bead radius for a single BZ hydrogel bead. (*B*) Image of collection of BZ hydrogel beads all smaller than $R_{c,exp}$, the critical radius for a single BZ hydrogel bead to oscillate. The deep and light orange BZ hydrogel beads are made with $[Ru^{2+}] = 15$ mM and $[Ru^{2+}] = 3$ mM respectively. The scale bar is 250 μm. (*C*) Ratio of period $\frac{T}{T_0}$ as a function of Ruthenium catalyst concentration in the steady state oscillation regime, i.e., when the period of oscillation is constant, for all BZ hydrogel bead sizes. T_0 is the mean oscillation period of the background BZ hydrogel beads with $[Ru^{2+}] = 3$ mM.

We now construct a reaction–diffusion theoretical model that qualitatively explains the three most salient features of our experiment: 1) Spherical BZ hydrogel beads smaller than a critical size $R_{c,exp}$ stay oxidized. Only above a critical radius $R_{c,exp}$, the BZ hydrogel beads chemically oscillate. 2) Adding neighboring BZ hydrogel beads all smaller than the critical size decreases the critical size for a BZ hydrogel bead to oscillate. 3) In the quorum-sensing regime with heterogeneous BZ hydrogel beads, the steady-state period of oscillation increases with their catalyst concentration.

The physics of an oscillating BZ gel in an uncatalyzed BZ solution is governed by reaction–diffusion processes. The variation over time of the concentration of BZ species $\frac{\partial c_i}{\partial t}$ is due to the diffusion of products in and out of the gel $D\Delta c_i$, with D the molecular diffusion coefficient, and the reaction rate $R(c_i)$ representing the kinetics of the BZ reactions. We simplify this spatially extended model to a point model by assuming the concentration of the BZ species in the BZ hydrogel c_i to be homogeneous and by writing the diffusion term $D\Delta c_i$ as $-\alpha_i c_i$. Hence,

$$\frac{dc_i}{dt} = -\alpha_i c_i + R(c_i). \quad [1]$$

To justify the mathematical expression of the loss term $-\alpha_i c_i$, consider the number of moles of a chemical product i inside a BZ gel $N_{i,in}$. This product is diffusing out of the gel with a flux j_i proportional to its concentration gradient, $j_i = -D\nabla c_i \sim D\frac{dc_i}{dx} \sim \beta_i c_i$, where $\beta_i = \frac{D}{L_i}$, with L_i the typical lengthscale over which the gradient is built across the surface of the bead. The variation of the number of moles of product inside the bead $dN_{i,in}$ due to its loss through its surface in contact with the uncatalyzed BZ solution can be written as $\frac{dN_{i,in}}{dt} = j_i S$, or equivalently as $\frac{d(Vc_i)}{dt} = -\beta_i c_i S$, where we have used that $N_{i,in} = V c_i$, with V the volume. Taking the size of a BZ hydrogel bead as constant, the temporal variation of the concentration of product i due to its outward flux becomes $\frac{dc_i}{dt} = -\beta_i \frac{S}{V} c_i$. The loss term then acts as an additional effective first-order chemical reaction on the temporal evolution of the chemical concentration. We define $\alpha_i = \beta_i \frac{S}{V} \propto \frac{D}{L_i}\frac{S}{V}$. The lengthscales L_i can be controlled by diffusion, reaction, and reaction-induced convection when the chemicals leaving the hydrogel react in the media outside the hydrogel (18, 22). If we assume that the chemical reactions do not induce convection in the uncatalyzed BZ solution and that these reactions can be modeled as first-order chemical reactions with kinetic constant K_i, the lengthscales L_i take the following expression $L_i = \sqrt{\frac{D}{K_i}}$. Hence, α_i can be different for each of the mobile species involved in the BZ reaction. In the following, we use the Vanag–Epstein model for the kinetics of the BZ reaction, encoded in the term $R(c_i)$ (23). The Vanag–Epstein (VE) model simplifies the BZ reaction to a model with only four variables, each representing a chemical concentration. The four concentration variables are $c_1 = [HBrO_2]$, $c_2 = [Br^-]$, $c_3 = [\text{oxidized catalyst}] = [Ru^{3+}]$ and $c_4 = [Br_2]$. $HBrO_2$, Br^-, and Br_2 are chemicals which can diffuse out of the gel, whereas the Ru^{3+} is bound to the gel. We thus define α_{Br_2}, α_{Br^-}, and α_{HBrO_2} (*Materials and Methods*, D). We note that while the behavior between different models of the BZ reaction is qualitatively similar, quantitative comparisons between most model simulations of the BZ reaction and experimental results have not been possible (24). Therefore, the quantitative model developed here is intended to reproduce qualitatively the experimental system. For simplicity, we also assume that $\alpha_{Br^-} = \alpha_{Br_2}$. Our results do not qualitatively depend on this assumption (*SI Appendix*, section 7).

With this model, we construct a phase diagram, reported in Fig. 3*A*, that captures the oscillation state of the BZ hydrogel bead in terms of the rate of loss of the inhibitors α_{Br^-}, α_{Br_2} and of the activator α_{HBrO_2}. We observe 3 regions: At high α_{HBrO_2}, the BZ hydrogel bead stays reduced, because the activator $HBrO_2$ diffuses faster than its production rate (red) preventing its autocatalysis to proceed; at high α_{Br^-} and below certain α_{HBrO_2} value, the BZ hydrogel bead stays oxidized, because the inhibitors Br^- and Br_2 diffuse faster than their reaction rates with the ruthenium catalyst (green); otherwise the BZ hydrogel bead oscillates (gray). In the same figure, a change in radius of a BZ hydrogel bead corresponds to a straight line with a slope given by the ratio of the two relevant lengthscales L_{HBrO_2} and L_{Br^-}. A decrease in the radius of the BZ hydrogel is equivalent to an increase in both α_{HBrO_2} and α_{Br^-}. We obtain that the

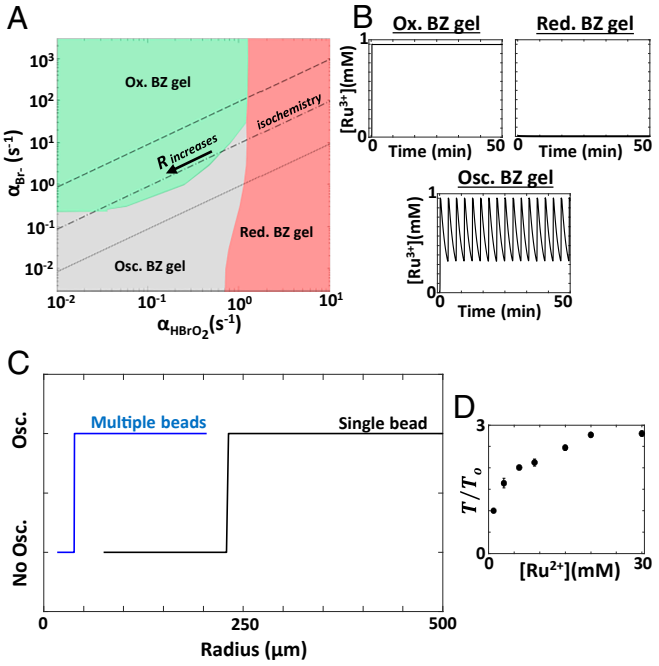

Fig. 3. Simulation results obtained with the theoretical reaction–diffusion model coupling the Vanag–Epstein model to additional loss terms of chemicals related diffusion or diffusion/reaction of chemicals. In all the simulations, $[Ru^{2+}]$ = 1 mM. (*A*) Phase diagram representing the chemical state of a BZ hydrogel bead as a function of the rates of loss of the activator, α_{HBrO_2}, and inhibitor α_{Br^-}. The green, red, and gray regions represent the states of the BZ hydrogel bead: oxidized, reduced, and oscillatory state, respectively. The dotted, dotted-dashed, and dashed lines correspond to a change in the radius of a BZ hydrogel bead. The slope corresponds to $\frac{L_{HBrO_2}}{L_{Br^-}} = 1$, $\frac{L_{HBrO_2}}{L_{Br^-}} = 10$, and $\frac{L_{HBrO_2}}{L_{Br^-}} = 100$ respectively. (*B*) Simulation results of an oxidized BZ hydrogel bead ($\alpha_{Br^-} = 1$; $\alpha_{HBrO_2} = 5 \times 10^{-2}$), of a reduced BZ hydrogel bead ($\alpha_{Br^-} = 1$; $\alpha_{HBrO_2} = 5$) and of an oscillating BZ hydrogel bead ($\alpha_{Br^-} = 1$; $\alpha_{HBrO_2} = 5 \times 10^{-1}$). (*C*) State of the oscillation of the BZ hydrogel bead as a function of its radius, for L_{HBrO_2} = 144 μm, L_{Br^-} = 34.6 μm, L_{Br_2} = 34.6 μm for an isolated BZ hydrogel bead (black line), for a collection of BZ hydrogel beads (blue line). We observe a transition from a nonoscillating oxidized to an oscillating BZ hydrogel bead when its radius increases. The theoretical critical size is $R_{c,theo}$ = 230 μm for an isolated gel and $R_{c,collective}$ = 38 μm for a gel in the collective regime. (*D*) Ratio of period $\frac{T}{T_0}$ as a function of the Ruthenium catalyst concentration in the steady state oscillation regime for $\beta = 0.002\,s^{-1}$.

ratio $\frac{L_{HBrO_2}}{L_{Br^-}}$ needs to be above 3.6 for a spherical BZ hydrogel to experience a transition from the oxidized state, when small, to the oscillatory state, when its radius is high (Fig. 3 *A* and *C* and *SI Appendix*, section 6). To find a theoretical critical size of $R_{c,theo} = 230\,\mu m$ consistent with the experimentally observed critical radius $R_{c,exp} = (225 \pm 9)\,\mu m$, we use the model with the set of lengthscales L_{HBrO_2} = 144 μm, L_{Br^-} = 34.6 μm = L_{Br_2}, resulting in $\frac{L_{HBrO_2}}{L_{Br^-}} = 4.16$. We verify that the numerical values for L_{HBrO_2}, L_{Br^-}, and L_{Br_2} are in reasonable agreement with the values of these lengthscales calculated from the rate constants of the reactions controlling the concentration profiles of these chemicals outside the BZ hydrogel bead. This is done by numerically integrating the Vanag–Epstein model when the catalyst concentration is set to 0 (*Material and Methods*, E). This theoretical analysis shows that L_{HBrO_2}, L_{Br^-}, and L_{Br_2} are all smaller than R_c. Thus, we find that for a BZ hydrogel bead with a radius R_c at the transition between oscillation and nonoscillation, the reaction rates of the chemicals set the lengthscale over which the chemicals diffuse out of the hydrogel, hence determining the magnitude of their outward flux.

To study the effect of neighboring BZ hydrogel beads on the chemical oscillation, we simulate a line of N hydrogels each affected by the reaction rates of the BZ reaction $R(c_{i,j})$, where $j = 1, ..., N$ labels the hydrogel bead in the line, and coupled chemically to each other and to the uncatalyzed BZ solution located at the top and side of the line by diffusion. The BZ hydrogel j is coupled to the outside BZ solution by a term $-\alpha_i c_{i,j}$, an expression we derived earlier for the single BZ hydrogel model. Additionally, the BZ hydrogel j is coupled to its closest neighbors $j-1$ and $j+1$ by the terms $-\beta(c_{i,j} - c_{i,j-1})$ and $-\beta(c_{i,j} - c_{i,j+1})$, respectively. These terms capture the diffusive flux of chemicals between neighboring BZ hydrogel beads (*Materials and Methods*, F). Solving numerically this system of $4 \times N$ nonlinear equations, we find that the critical size for an assembly of BZ hydrogel beads to oscillate is $R_{c,collective} = 38\,\mu m$ for all β and N values tested. $R_{c,collective}$ is 6 times smaller than the critical size for the single BZ hydrogel bead to oscillate (Fig. 3*C*). This result qualitatively reproduces the experimentally observed decrease in the critical size for a BZ hydrogel bead to oscillate in the collective regime. We can recover the same result with a model that considers a 2D layer of BZ hydrogel beads as a BZ hydrogel sheet. The loss terms $-\alpha_i$ are proportional to the BZ hydrogel bead surface-to-volume ratio $\frac{S}{V}$. For a sphere of radius R, $\frac{S}{V} = \frac{3}{R}$, whereas for a sheet made of close-packed spherical hydrogels of radius R , $\frac{S}{V} = \frac{1}{2R}$. Hence, $\frac{S}{V}|_{sphere} = 6\frac{S}{V}|_{sheet}$. The critical radius for a BZ hydrogel sheet to oscillate is expected to be $R_{c,sheet} = \frac{1}{6}R_{c,sphere}$ = 38 μm, in agreement with the numerical result obtained from the model with N coupled BZ hydrogel beads.

The model with N BZ hydrogel beads also allows simulating the experiments conducted with BZ hydrogel beads containing a heterogeneous catalyst concentration (Fig. 2*B*). We assume that the parameters $\alpha_{i,j}$ are independent of the catalyst concentration. In Fig. 3*D*, we show that the continuous increase in the oscillation period with catalyst concentration observed experimentally can be qualitatively reproduced in the simulations when the coupling $\beta \leq 0.002\,s^{-1}$. For stronger coupling between neighboring gels, an increase in the oscillation period with the catalyst concentration is also observed, but this increase appears quantized. In this case, $T_{c_{Ru^{2+},high}} = n \times T_{c_{Ru^{2+},low}}$, with $n \in \mathbb{N}$.

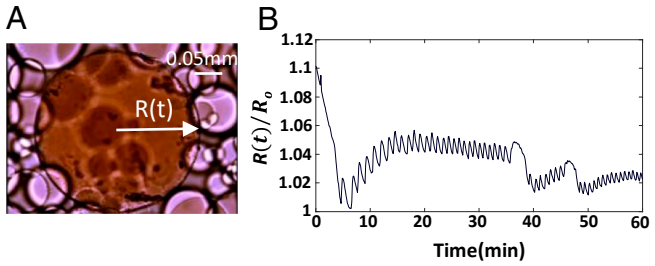

Fig. 4. Mechanical oscillation of a BZ hydrogel bead with a radius R = 150 μm smaller than the critical size $R_{c,exp}$ = 225 ± 9 μm embedded in a layer of BZ hydrogel beads. (*A*) Picture of a chemomechanical BZ hydrogel bead (dark orange), with $[Ru^{2+}]$ = 6 mM and a bulk modulus of 10 kPa, surrounded by smaller BZ chemically active hydrogel beads. (*B*) Relative radius change of a BZ chemomechanical hydrogel bead as a function of time.

3. Collective Chemomechanical Oscillations of BZ Hydrogel Beads

To end, we use the collective regime to study the occurrence of chemomechanical oscillations of specific BZ hydrogel beads with radii also below the critical radius $R_{c,exp}$. These specific BZ hydrogel beads are softer than the rest (bulk modulus ∼10 kPa) (18). We find that during an initial transient regime corresponding to a long period of chemical oscillation, such BZ hydrogel beads present mechanical oscillation of a few percent in strain (Movie S3 and *SI Appendix*, section 8). Their chemical oscillations eventually stabilize to a steady state regime with a faster oscillation period. We have observed that a 150-μm-radius BZ hydrogel bead mechanically oscillates in its steady state regime, with an amplitude of around 1% (Fig. 4 and Movie S4). Taken together, these experimental results demonstrate that the collective regime can be leveraged to trigger the chemomechanical oscillation of softer BZ hydrogels.

Using collective effects to change the critical size for a BZ hydrogel bead to chemically oscillate appears as a promising strategy to increase the oscillatory strain. Indeed, as the timescale of swelling of a spherical hydrogel is proportional to the square of its size (25), we hypothesize that decreasing further the size of a BZ hydrogel embedded in this assembly should increase its chemomechanical energy conversion. Future work will consist in testing this idea by tuning the size and environment of BZ hydrogel beads.

4. Conclusion and Outlook

We have shown that the collective chemical response of an assembly of soft BZ hydrogel beads triggers their chemomechanical oscillations. A single spherical BZ hydrogel smaller than a critical radius $R_{c,exp}$ does not chemically oscillate because it stayed oxidized. This is in stark contrast to previous results on the oscillation behavior of catalyst-loaded particles for which the catalyst stays reduced. We then construct a model of the BZ hydrogel bead coupled to its outside environment through diffusion that reproduces this experimental observation. The theory indicates that this size-dependent behavior is due to a competition between the reaction kinetics of the inhibitor of the BZ reaction and its transport to the outer solution. With both experiment and theory, we also show that an assembly of close-packed BZ hydrogel beads with a radius smaller than the previously established critical size for a single BZ hydrogel to oscillate can sustain chemical oscillation. In this collective regime, BZ hydrogel beads, tuned in composition to improve their oscillation strain, are now mechanically active.

These results are important for optimizing the performance of autonomous chemomechanical machines. Indeed, they highlight the role of the size of a BZ hydrogel bead and the role of its environment on its chemomechanical properties. They demonstrate that it is possible to design a multiscale material made with a first lengthscale controlling the mechanical swelling timescale and a second lengthscale dictating the chemical oscillation of the gel. It also shines light on previous experiments made with BZ gels, emulsions or coacervates at the nano/micro scale (26). For example, recent experimental results demonstrate that BZ polymeric shells of around 20 μm in diameter undergo buckling unbuckling instabilities (27) and that BZ coacervates or BZ microgels of around 1 μm in diameter sustain chemomechanical oscillations (28, 29). Our interpretation of these results is that the oscillations of such small polymeric BZ microreactors might be the result of a collective chemical response. Provided that the density of these BZ microcompartments in the solution is high enough, they can exchange chemicals which can trigger their collective chemomechanical oscillation. Also, in the collective regime, if each BZ hydrogel bead is viewed as a unit cell, our work is a step toward the creation of the recently called "swarmalator," a model system consisting of a swarm of autonomous chemically communicating chemomechanical oscillators (19, 30–32). Indeed each BZ hydrogel bead consumes chemical energy to communicate with its neighbor and actuate mechanically. The remaining challenge to achieve this goal is to convert its mechanical actuation into motion. The self-propulsion of an autonomous BZ bilayer hydrogel has been experimentally demonstrated by patterning the substrate with a sawtooth design to guide the motion of the BZ bilayer in a specific direction (33). Theoretical work also shows that directed motion can be obtained by adding a gradient of adhesion force between the substrate and the BZ hydrogel (32). In these scenarios, the direction of the BZ gel motion is controlled by the anisotropy of the surface interacting with the BZ gel and is therefore not intrinsic to the BZ gel material itself. As a result, the BZ gel direction cannot adapt to external stimuli such as the chemical gradient generated by neighboring BZ gels. Nonetheless, from these experiments, we can calculate the typical Reynolds number of such BZ gel walkers moving in water. With a speed u = 1 μm s^{-1}, a size L = 1 cm, and $\nu = 10^{-6}\mathrm{m}^2\,\mathrm{s}^{-1}$ the kinematic viscosity of water, we get $Re = \frac{uL}{\nu} \sim 0.01$. At low Reynolds numbers, the self-propulsion is notably hard because breaking time-reversal symmetry is needed to swim (34, 35). The presence of nonlinearity in both mechanics and the BZ chemistry as well as the many degrees of freedom offered by the softness of the hydrogels should facilitate nonreciprocal back and forth motions, hence promoting motility (36–38). Moreover, biology provides examples of organisms that can move at low Reynolds numbers. Those called euglenids harness self-propagating waves directed along their body to move (39, 40). Theoretical work confirms that an active actomyosin network or a BZ chemical reaction on a deformable membrane display autonomous shape changes including a buckling instability that can ultimately lead to motility (41–43). Motile soft robots have also been engineered from 2D membranes powered with a magnetic field (44–46). Therefore, as a first step, 2D shape-changing hydrogels, which have been developed recently, could be made BZ active to generate autonomous folding-unfolding of their structure (47, 48). Further work will then be needed to convert a cyclic shape-changing BZ hydrogel into a self-propelled BZ hydrogel. Taken together, our work opens different directions in the study of the collective behavior of life-like materials, from their locomotion to their self-assembly. Working with a model system such as BZ hydrogels can also help rationalize how multicellular organization emerges as a result of chemical cues and chemomechanical energy conversion at the molecular level.

5. Materials and Methods

A. Materials. Acrylamide (AAm) (99.9%), 1-ethyl-3-(3-(dimethylamino)propyl) carbodiimide HCl (EDC), N-hydroxysuccinimide (NHS), 2-(4-morpholino) ethanesulfonic acid (MES), hexadecane, 2-propanol, sodium phosphate monobasic anhydrous (99%), sodium phosphate dibasic anhydrous (≥ 99%), Tween 20, poly(dimethylsiloxane) (PDMS) elastomer kits (Sylgard 184), and sodium hydroxide (NaOH) were purchased from Thermo Fisher Scientific (Waltham, MA). Acrylic acid (AAc) anhydrous (180 to 200 ppm MEHQ inhibitor,99%), 2-hydroxy-2-methylpropiophenone (Darocur 1173, photoinitiator), saline sodium citrate (SSC) buffer (20- concentrate, molecular biology grade), N-Boc ethylene diamine, hydroxybenzotriazole (HOBt), N,N-dimethylformamide (DMF), Tetrahydrofuran (THF), N,N′-Diisopropylcarbodiimide (DIC) and N,N′-Methylenebis(acrylamide) (Bis) were purchased from Sigma-Aldrich. 4-Methyl-4′-carboxy-2,2′-bipyridine was purchased from Carbosynth. All chemicals were of analytical grade and used without further purification.

B. BZ Hydrogel Beads Fabrication. The p(AAm-co-AA) microspheres in this study were fabricated according to methods in recent reports (20). Briefly, the compositions of the aqueous prepolymer solutions were 15% (w/v) AAm, 0.5 to 10% (w/v) AAc, 0.05 to 1% (w/v) Bis, and the composition of the wetting fluid was 99% (v/v) hexadecane and 1% (v/v) Darocur 1173 photoinitiator. The prepolymer solution was placed into a micropatterned PDMS mold, which was formed with Sylgard 184 containing 10% (w/w) curing agent following overnight incubation at 65 °C on a silicon master template. Excess prepolymer solution was removed via pipetting, and the wetting fluid was then placed on top of the mold in order to lead to surface tension-induced droplet formation. The mold was then carefully placed on an aluminum mirror (Thorlabs, Newton, NJ) and exposed to low-intensity 365 nm UV light with an 8 W hand-held UV lamp (Spectronics Corp., Westbury, NY) for 15 min to initiate radical chain polymerization. The microspheres were collected via pipetting, transferred to a microcentrifuge tube, and rinsed to remove any wetting fluid and unreacted chemicals as follows: mixing the microspheres in 2-propanol by pipetting, allowing them to settle to the bottom, and removing the supernatant. After rinsing at least three times with 2-propanol, the rinsing procedure was repeated at least three times with deionized water containing 0.05% (v/v) Tween 20 and at least twice with 20 mM MES buffer (adjusted to pH 6 with 1 M NaOH) containing 0.05% (v/v) Tween 20 or deionized water.

To fabricate p(AAm-co-AA) polydisperse microbeads, we used an oil-in-water emulsion approach (21). By vortexing the two phases, a dispersion of water droplets was formed in the oil phase. RAN Biotechnologies FluoroSurfactant stabilized oil (3MTM NovecTM 7500 Engineered Fluid) was used as the oil phase. The polymer solution and the oil are purged with nitrogen. Once the emulsion was formed, it was also purged for 5 min with nitrogen, and then let to polymerize overnight at 60 °C under nitrogen atmosphere to produce spherical microbeads. To transfer the microbeads into PBS, we used perfluorooctanol (PFO, Sigma 370533). On the top of the emulsion, 500 ml of PBS was gently added. Subsequently, 400 ml of PFO was poured into the mix. By pipetting the PBS phase, beads were transferred into the water phase and then thoroughly washed with PBS to remove excess of non-cross-linked acrylamide monomers.

The ruthenium catalyst is synthesized in our lab following our previous procedure (18). We recall briefly the procedure here. The starting material 4-Methyl-4′-carboxy-2,2′-bipyridine is commercially available from Carbosynth. The 4-Methyl-4′-carboxy-2,2′-bipyridine is activated with N-Hydroxysuccinimide. The fresh NHS ester is then added to N-Boc ethylene diamine. Excess of trifluoroacetic acid is added to the mixture to remove the Boc protecting group to obtain the ligand 4-methyl-4-amido ethylamine-2,2′-bipyridine as white solid via HPLC purification. The ligand is then mixed with cis–dichlorobis(2,2′–bipyridine)ruthenium(II). The mixture was distilled in darkness for 3 d. After removing the solvent, NH_4PF_6 solution is added into the residue and a red

precipitate is collected and washed with cold water. The ruthenium catalyst is obtained through purification of the red precipitate on a Sephadex-LH 20 column.

The hydrogel beads are functionalized with the ruthenium catalyst via carbodiimide chemistry. First, 400 mM EDC and 100 mM NHS are added to microspheres in 20 mM MES buffer (pH 6) containing 0.05% (v/v) Tween 20, mixed via pipetting, and placed on a rotator for 15 min at room temperature. Then, unreacted EDC and NHS are removed by rinsing the microspheres with 20 mM MES buffer (pH 6) containing 0.05% (v/v) Tween 20 at least three times and then 100 mM sodium phosphate buffer adjusted to pH 8 by adding 1M of NaOH solution, at least twice. For ruthenium catalyst conjugation, p(AAm-co-AAc) microspheres activated with EDC/NHS are reacted with 10 μL of a solution of 35 mM ruthenium catalyst dissolved in DMF in 100 μL of bead solution overnight on a rotator at room temperature in the sodium phosphate buffer adjusted to pH 8. Unreacted ruthenium BZ catalyst molecules are removed by rinsing the microspheres 3 times with deionized water+0.05% (v/v) and at least 3 times with 5×SSC buffer (pH 7) containing 0.05% (v/v) Tween 20.

C. Experimental Setup for Characterizing the Oscillating BZ Hydrogel Beads. Each experiment is conducted in a container made of a glass slide at the bottom and at the top, with a PDMS lateral wall of approximately 5 mm in height and 1 cm in diameter. The solution is kept under pressure with a clamp to avoid evaporation and the creation of carbon dioxide bubbles. The change in color of the catalyst is recorded as a function of time. Ruthenium-conjugated microspheres were visualized with an epifluorescence microscope (Olympus BX51 equipped with a DP70 microscope digital camera, Center Valley, PA) or a Leica S4 E Stereo Zoom Microscope with a MARLIN F-131C color camera. The images were then analyzed with MATLAB software to obtain the temporal evolution of the intensity and the radius change of a gel.

D. Vanag–Epstein Model with Additional Loss Terms. The Vanag–Epstein (VE) model simplifies the BZ reaction to a model with only four variables, each representing a chemical concentration. The four concentration variables are $c_1 = [HBrO_2]$, $c_2 = [Br^-]$, $c_3 = [\text{oxidized catalyst}] = [Ru^{3+}]$, and $c_4 = [Br_2]$. $HBrO_2$, Br^-, and Br_2 are chemicals which can diffuse out of the gel, whereas the oxidized catalyst Ru^{3+} is bound to the gel. We thus define α_{Br_2}, α_{Br^-}, and α_{HBrO_2}, the loss terms of Br_2, Br^-, and $HBrO_2$, respectively. The four equations in the model are:

$$\frac{dc_1}{dt} = -k_1c_1c_2 + k_2c_2 - 2k_3c_1^2 + k_4c_1\frac{(c_{3,0}-c_3)}{c_{3,0}-c_3+c_{\min}} - \alpha_{HBrO_2}c_1,$$

$$\frac{dc_2}{dt} = -3k_1c_1c_2 - 2k_2c_2 - k_3c_1^2 + k_7c_4 + k_9c_3 - \alpha_{Br^-}c_2,$$

$$\frac{dc_3}{dt} = 2k_4c_1\frac{(c_{3,0}-c_3)}{c_{3,0}-c_3+c_{min}} - k_9c_3 - k_{10}c_3,$$

$$\frac{dc_4}{dt} = 2k_1c_1c_2 + k_2c_2 + k_3c_1^2 - k_7c_4 - \alpha_{Br_2}c_4.$$

The rate constants of the reactions, k_i, and the constant concentration $c_{\min}$ are given in *SI Appendix*, section 1.

We solve this coupled nonlinear differential equation using the MATLAB solver ode15.

E. Calculating the Lengthscale over which the Intermediates of the BZ Reaction Diffuse. The physics governing the concentration profile of chemicals synthesized in BZ gel diffusing to its surroundings is captured by a reaction–diffusion model. The variation over time of the concentration of the BZ species is due to the diffusion of product, $D\Delta c$, and the reaction rate, $R(c)$, encoding the kinetics of the BZ reactions. Explicitly,

$$\frac{\partial c}{\partial t} = D\Delta c + R(c). \quad [2]$$

To calculate a profile of chemicals, we integrate this equation in 1 dimension, when the gel is stuck in the oxidized state. Hence, the concentrations of the chemicals c_i are stationary in time. The boundary condition on the concentration is taken from the value given by the point model described in *Materials and Methods*, D at the transition between the oscillating and oxidized states. We solve this coupled nonlinear differential equation using the MATLAB solver ode15. We fit the numerical profile of each chemicals $HBrO_2$, Br^-, and Br_2 with an exponential function to extract the lengthscales L_{HBrO_2}, L_{Br^-}, and L_{Br_2}, respectively (*SI Appendix*, section 6).

F. Simulating a Line of N BZ Chemical Oscillator Coupled by Diffusion. We simulate a line of N gels coupled chemically by diffusion with their lateral neighbors. Each BZ bead is indexed by the letter j that represents its spatial position. Its neighbors are in $j-1$ and $j+1$. The BZ reaction is modeled with a VE model, with a loss term α_i that accounts for its coupling with the uncatalyzed BZ solution and with a coupling term between BZ neighboring hydrogels captured by a coefficient β_j. α_i are chosen according to the chemical profile of mobile species in the BZ reaction and the surface to volume ratio of the BZ hydrogel bead exposed to the solution. i represents the four chemical species involved in the Vanag–Epstein model with $c_1 = [HBrO_2]$, $c_2 = [Br^-]$, $c_3 = [\text{oxidized catalyst}] = [Ru^{3+}]$, and $c_4 = [Br_2]$. β_j is a free parameter. We solve the following system of equations using the MATLAB solver ode15 for j going for 2 to $N-1$.

$$\frac{dc_{1,j}}{dt} = -k_1c_{1,j}c_{2,j} + k_2c_{2,j} - 2k_3c_{1,j}^2 + k_4c_{1,j}\frac{(c_{3,0,j}-c_{3,j})}{c_{3,0,j}-c_{3,j}+c_{\min,j}} - \alpha_{HBrO_2}c_{1,j} - \beta(2c_{1,j}-c_{1,j-1}-c_{1,j+1}),$$

$$\frac{dc_{2,j}}{dt} = -3k_1c_{1,j}c_{2,j} - 2k_2c_{2,j} - k_3c_{1,j}^2 + k_7c_{4,j} + k_9c_{3,j} - \alpha_{Br^-}c_{2,j} - \beta(2c_{2,j}-c_{2,j-1}-c_{2,j+1}),$$

$$\frac{dc_{3,j}}{dt} = 2k_4c_{1,j}\frac{(c_{3,0,j}-c_{3,j})}{c_{3,0,j}-c_{3,j}+c_{\min,j}} - k_9c_{3,j} - k_{10}c_{3,j},$$

$$\frac{dc_{4,j}}{dt} = 2k_1c_{1,j}c_{2,j} + k_2c_{2,j} + k_3c_{1,j}^2 - k_7c_{4,j} - \alpha_{Br_2}c_{4,j} - \beta(2c_{4,j}-c_{4,j-1}-c_{4,j+1}),$$

with the additional equations for bead 1 and N:

$$\frac{dc_{1,1}}{dt} = -k_1c_{1,1}c_{2,1} + k_2c_{2,1} - 2k_3c_{1,1}^2 + k_4c_{1,1}\frac{(c_{3,0,1}-c_{3,1})}{c_{3,0,1}-c_{3,1}+c_{\min,1}} - 2\alpha_{HBrO_2}c_{1,1} - \beta(c_{1,1}-c_{1,2}),$$

$$\frac{dc_{2,1}}{dt} = -3k_1c_{1,1}c_{2,1} - 2k_2c_{2,1} - k_3c_{1,1}^2 + k_7c_{4,1} + k_9c_{3,1} - 2\alpha_{Br^-}c_{2,1} - \beta(c_{2,1}-c_{2,2}),$$

$$\frac{dc_{3,1}}{dt} = 2k_4c_{1,1}\frac{(c_{3,0,1}-c_{3,1})}{c_{3,0,1}-c_{3,1}+c_{\min,1}} - k_9c_{3,1} - k_{10}c_{3,1},$$

$$\frac{dc_{4,j}}{dt} = 2k_1c_{1,1}c_{2,1} + k_2c_{2,1} + k_3c_{1,1}^2 - k_7c_{4,1} - 2\alpha_{Br_2}c_{4,1} - \beta(c_{4,1}-c_{4,2}).$$

$$\frac{dc_{1,N}}{dt} = -k_1c_{1,N}c_{2,N} + k_2c_{2,N} - 2k_3c_{1,N}^2 + k_4c_{1,N}\frac{(c_{3,0,N}-c_{3,N})}{c_{3,0,N}-c_{3,N}+c_{\min,N}} - 2\alpha_{HBrO_2}c_{1,N}$$

$$- \beta(c_{1,N} - c_{1,N-1}),$$

$$\frac{dc_{2,N}}{dt} = -3k_1 c_{1,N} c_{2,N} - 2k_2 c_{2,N} - k_3 c_{1,N}^2 + k_7 c_{4,N} + k_9 c_{3,N} - 2\alpha_{Br^-} c_{2,N} - \beta(c_{2,N} - c_{2,N-1}),$$

$$\frac{dc_{3,N}}{dt} = 2k_4 c_{1,N} \frac{(c_{3,0,N} - c_{3,N})}{c_{3,0,N} - c_{3,N} + c_{\min,N}} - k_9 c_{3,N} - k_{10} c_{3,N},$$

$$\frac{dc_{4,N}}{dt} = 2k_1 c_{1,N} c_{2,N} + k_2 c_{2,N} + k_3 c_{1,N}^2 - k_7 c_{4,N} - 2\alpha_{Br_2} c_{4,N} - \beta(c_{4,N} - c_{4,N-1}).$$

Data, Materials, and Software Availability. The data are available in the public depository Zenodo (https://doi.org/10.5281/zenodo.10467546)(49). All other data are included in the article and/or supporting information.

ACKNOWLEDGMENTS. We thank M. Deforet for critical readings of the manuscript. B.B acknowledges support of the Brandeis Provost research award, the Council for the Arts at Massachusetts Institute of Technology (CAMIT) grant from Massachusetts Institute of Technology (MIT), the financial help from Somerville Art Council, the Maria Zambrano fellowship from the University of Barcelona, and funding from the European Union's Horizon 2020 research and innovation program under the Marie Sklodowska-Curie grant agreement COFUND Prg Autopo REGION Ile de France (IDF). A.F.-N. thanks MCIN/AEI/10.13039/501100011033/FEDER, UE (grant No. PID2021-122369NB-I00) for financial support.

Author affiliations: [a]Laboratoire Jean Perrin, Sorbonne Université, CNRS, Institut de Biologie Paris-Seine (IBPS), Paris 75005, France; [b]Department of Condensed Matter Physics, University of Barcelona, Barcelona 08028, Spain; [c]Department of Physics, Brandeis University, Waltham, MA 02454; [d]Department of Biomedical and Chemical Engineering, Syracuse University, Syracuse, NY 13244; [e]Institute of Complex Systems, University of Barcelona, Barcelona 08028, Spain; and [f]Institució Catalanade Recerca i Estudis Avançats, Barcelona 08010, Spain

1. J. Gautrais *et al.*, Deciphering interactions in moving animal groups. *PLoS Comput. Biol.* **8**, e1002678 (2012).
2. G. Bub, A. Shrier, L. Glass, Global organization of dynamics in oscillatory heterogeneous excitable media. *Phys. Rev. Lett.* **94**, 028105 (2005).
3. R. D. Vale, The molecular motor toolbox for intracellular transport. *Cell* **112**, 467–480 (2003).
4. R. Alert, X. Trepat, Physical models of collective cell migration. *Annu. Rev. Condens. Matter Phys.* **11**, 77–101 (2020).
5. J. Li, S. K. Schnyder, M. S. Turner, R. Yamamoto, Role of the cell cycle in collective cell dynamics. *Phys. Rev. X* **11**, 031025 (2021).
6. J. A. Acebrón, L. L. Bonilla, C. J. P. Vicente, F. Ritort, R. Spigler, The Kuramoto model: A simple paradigm for synchronization phenomena. *Rev. Mod. Phys.* **77**, 137 (2005).
7. M. A. Munoz, Colloquium: Criticality and dynamical scaling in living systems. *Rev. Mod. Phys.* **90**, 031001 (2018).
8. T. Gregor, K. Fujimoto, N. Masaki, S. Sawai, The onset of collective behavior in social amoebae. *Science* **328**, 1021–1025 (2010).
9. D. G. Davies *et al.*, The involvement of cell-to-cell signals in the development of a bacterial biofilm. *Science* **280**, 295–298 (1998).
10. C. M. Waters, B. L. Bassler, Quorum sensing: Cell-to-cell communication in bacteria. *Annu. Rev. Cell Dev. Biol.* **21**, 319–346 (2005).
11. A. F. Taylor, M. R. Tinsley, F. Wang, Z. Huang, K. Showalter, Dynamical quorum sensing and synchronization in large populations of chemical oscillators. *Science* **323**, 614–617 (2009).
12. R. Toth, A. F. Taylor, M. R. Tinsley, Collective behavior of a population of chemically coupled oscillators. *J. Phys. Chem. B* **110**, 10170–10176 (2006).
13. M. R. Tinsley, A. F. Taylor, Z. Huang, F. Wang, K. Showalter, Dynamical quorum sensing and synchronization in collections of excitable and oscillatory catalytic particles. *Phys. D: Nonlinear Phen.* **239**, 785–790 (2010).
14. M. R. Tinsley, A. F. Taylor, Z. Huang, K. Showalter, Emergence of collective behavior in groups of excitable catalyst-loaded particles: Spatiotemporal dynamical quorum sensing. *Phys. Rev. Lett.* **102**, 158301 (2009).
15. G. Gines *et al.*, Microscopic agents programmed by DNA circuits. *Nat. Nanotechnol.* **12**, 351–359 (2017).
16. A. M. Zhabotinsky, Periodic liquid phase reactions. *Proc. Acad. Sci. USSR* **157**, 392–395 (1964).
17. R. Yoshida, T. Takahashi, T. Yamaguchi, H. Ichijo, Self-oscillating gel. *J. Am. Chem. Soc.* **118**, 5134–5135 (1996).
18. B. Blanc *et al.*, Active gels: From chemical microreactor to polymeric actuator. arXiv [Preprint] (2022). http://arxiv.org/abs/2201.08273 (Accessed 20 January 2022).
19. K. P. O'Keeffe, H. Hong, S. H. Strogatz, Oscillators that sync and swarm. *Nat. Commun.* **8**, 1504 (2017).
20. E. Y. Liu, S. Jung, H. Yi, Improved protein conjugation with uniform, macroporous poly (acrylamide-co-acrylic acid) hydrogel microspheres via EDC/NHS chemistry. *Langmuir* **32**, 11043–11054 (2016).
21. M. E. Dolega *et al.*, Cell-like pressure sensors reveal increase of mechanical stress towards the core of multicellular spheroids under compression. *Nat. Commun.* **8**, 14056 (2017).
22. M. Menzinger, A. Tzalmona, R. L. Armstrong, A. Cross, C. Lemaire, Dynamics of convective instability of waves in the Belousov-Zhabotinskii reaction as measured by magnetic resonance imaging. *J. Phys. Chem.* **96**, 4725–4727 (1992).
23. V. K. Vanag, I. R. Epstein, A model for jumping and bubble waves in the Belousov-Zhabotinsky-aerosol OT system. *J. Chem. Phys.* **131**, 104512 (2009).
24. D. Wilson, S. Faramarzi, J. Moehlis, M. R. Tinsley, K. Showalter, Synchronization of heterogeneous oscillator populations in response to weak and strong coupling. *Chaos: Interdisc. J. Nonlinear Sci.* **28**, 123114 (2018).
25. M. Doi, Gel dynamics. *J. Phys. Soc. Jpn.* **78**, 052001 (2009).
26. R. Yoshida, Self-oscillating gels driven by the Belousov-Zhabotinsky reaction as novel smart materials. *Adv. Mater.* **22**, 3463–3483 (2010).
27. R. Tamate, T. Ueki, R. Yoshida, Self-beating artificial cells: Design of cross- linked polymersomes showing self-oscillating motion. *Adv. Mater.* **27**, 837–842 (2015).
28. Y. Yan *et al.*, Dynamical behaviors of oscillating metallosurfactant coacervate microdroplets under redox stress. *Adv. Mater.* **35**, e2210700 (2023).
29. K. Inui *et al.*, The Belousov-Zhabotinsky reaction in thermoresponsive core-shell hydrogel microspheres with a Tris (2, 2″-bipyridyl) ruthenium catalyst in the core. *J. Phys. Chem. B* **124**, 3828–3835 (2020).
30. P. Dayal, O. Kuksenok, A. C. Balazs, Reconfigurable assemblies of active, autochemotactic gels. *Proc. Natl. Acad. Sci. U.S.A.* **110**, 431–436 (2013).
31. O. Kuksenok *et al.*, Chemo-responsive, self-oscillating gels that undergo biomimetic communication. *Chem. Soc. Rev.* **42**, 7257–7277 (2013).
32. G. V. Kolmakov, V. V. Yashin, S. P. Levitan, A. C. Balazs, Designing communicating colonies of biomimetic microcapsules. *Proc. Natl. Acad. Sci. U.S.A.* **107**, 12417–12422 (2010).
33. S. Maeda, Y. Hara, T. Sakai, R. Yoshida, S. Hashimoto, Self' walking gel. *Adv. Mater.* **19**, 3480–3484 (2007).
34. E. Lauga, T. R. Powers, The hydrodynamics of swimming microorganisms. *Rep. Progr. Phys.* **72**, 096601 (2009).
35. E. M. Purcell, Life at low Reynolds number. *Am. J. Phys.* **45**, 3–11 (1977).
36. C. Wischnewski, J. Kierfeld, Snapping elastic disks as microswimmers: Swimming at low Reynolds numbers by shape hysteresis. *Soft Matter* **16**, 7088–7102 (2020).
37. L. Ren *et al.*, Chemomechanical origin of directed locomotion driven by internal chemical signals. *Sci. Adv.* **6**, eaaz9125 (2020).
38. T. Yang *et al.*, Reconfigurable microbots folded from simple colloidal chains. *Proc. Natl. Acad. Sci. U.S.A.* **117**, 18186–18193 (2020).
39. G. Noselli, A. Beran, M. Arroyo, A. DeSimone, Swimming Euglena respond to confinement with a behavioural change enabling effective crawling. *Nat. Phys.* **15**, 496–502 (2019).
40. M. Arroyo, L. Heltai, D. Millán, A. DeSimone, Reverse engineering the euglenoid movement. *Proc. Natl. Acad. Sci. U.S.A.* **109**, 17874–17879 (2012).
41. S. Li, D. A. Matoz-Fernandez, A. Aggarwal, M. O. de la Cruz, Chemically controlled pattern formation in self-oscillating elastic shells. *Proc. Natl. Acad. Sci. U.S.A.* **118**, e2025717118 (2021).
42. A. Mietke, F. Jülicher, I. F. Sbalzarini, Self-organized shape dynamics of active surfaces. *Proc. Natl. Acad. Sci. U.S.A.* **116**, 29–34 (2019).
43. A. Zakharov, K. Dasbiswas, Mechanochemical induction of wrinkling morphogenesis on elastic shells. *Soft Matter* **17**, 4738–4750 (2021).
44. W. Hu, G. Lum, M. Mastrangeli, M. Sitti, Small-scale softbodied robot with multimodal locomotion. *Nature (London)* **81**, 554 (2018).
45. C. Li *et al.*, Fast and programmable locomotion of hydrogel-metal hybrids under light and magnetic fields. *Sci. Robot.* **5**, eabb9822 (2020).
46. C. A. Brisbois, M. O. De La Cruz, Locomotion of magnetoelastic membranes in viscous fluids. *Phys. Rev. Res.* **4**, 023166 (2022).
47. P. Techawanitchai *et al.*, Photo-switchable control of pH-responsive actuators via pH jump reaction. *Soft Matter* **8**, 2844–2851 (2012).
48. J. H. Na *et al.*, Programming reversibly self-folding origami with micropatterned photo-crosslinkable polymer trilayers. *Adv. Mater.* **27**, 79–85 (2015).
49. B. Blanc *et al.*, Collective chemomechanical oscillations in active hydrogels. Zenodo. https://zenodo.org/records/10467546. Deposited 8 January 2024.